From metastability to equilibrium during the sequential growth of Co–Ag supported clusters: a real-time investigation

Pascal Andreazza, A. Lemoine, A. Coati, D. Nelli, R. Ferrando, Y. Garreau, J. Creuze, C. Andreazza-Vignolle

Journal Name

ARTICLE TYPE

Cite this: DOI: 00.0000/xxxxxxxxxx

From metastability to equilibrium during the sequential growth of Co-Ag supported clusters: a real-time investigation†

P. Andreazza,*[a] A. Lemoine,[a,b], A. Coati,[b] D. Nelli,[c] R. Ferrando,[c] Y. Garreau,[d] J. Creuze,[e] and C. Andreazza-Vignolle[a]

Received Date
Accepted Date

DOI: 00.0000/xxxxxxxxxx

Atomic motions and morphological evolution of growing Co-Ag nanoparticles are followed in situ and in real time, by wide and small angle X-ray scattering obtained simultaneously in grazing incidence geometry (GISAXS and GIWAXS), in single or multi-wavelength (anomalous) modes. The structural analysis of the experimental data is performed with the aid of equilibrium Monte Carlo simulations and of molecular-dynamics simulations of nanoparticle growth. Growth is performed by depositing Co atoms above preformed Ag nanoparticles. This growth procedure is strongly out of equilibrium, because Ag tends to surface segregation, and generates complex growth sequences. The real time analysis of the growth allows to follow the nanoparticle evolution pathways almost atom-by-atom, determining the key mechanisms by which the nanoparticles finally approach their equilibrium core-shell and quasi-Janus structures.

1 Introduction

Bimetallic nanoparticles (often called nanoalloys) present a wide range of tunable properties, which stem to a large extent from their variety of chemical ordering types[1,2], ranging from fully mixed to completely segregated[1,3]. Mixed alloys can be either random or ordered, with several possible types of ordering[4–7] whereas segregated nanoalloys comprise core-shell (also with incomplete shells), multishell and Janus particles[8–14].

When the components are weakly miscible (as for example in Cu-Ag, Ni-Ag, Co-Ag, Co-Au and many others[1]) core-shell and Janus or quasi-Janus patterns are expected at equilibrium. In core-shell nanoalloys, a shell of the surface-segregating element A covers a core of the other element B, indicated as B@A. In quasi-Janus structures, the core is in off-center position, so that it is covered by a very thin layer of the shell element on one of its sides[15–18].

Here we focus on Co-Ag, a system combining very interesting magnetic and plasmonic effects[19,20]. Co-Ag is weakly miscible in bulk samples, with a miscibility gap for almost all compositions in the bulk solid phase[21]. Ag is less cohesive (E_{coh}^{Ag} = 2.95 eV/at, E_{coh}^{Co} = 4.45 eV/at[15]), has a much lower surface energy (E_S^{Ag} = 553 meV/at, E_S^{Co} = 961 meV/at[22]) and larger atom size than Co ($r_{Ag}/r_{Co} = 1.185$). All these factors are in favor of phase separation with strong Ag surface segregation in Co-Ag nanoparticles[1].

Theoretical studies on Co-Ag nanoparticles[15–17,23,24] showed equilibrium phase separation down to the nanoscale. For Ag-rich compositions, clustering of Co atoms in sub-surface positions was obtained in fcc and decahedral structures, whereas in icosahedra (Ih) Co atoms occupied central sites. With increasing Co content, larger off-center Co cores were formed (quasi-Janus structures), which progressively extend to the center of the nanoparticle, leading to a transition from quasi-Janus to Co@Ag. The picture arising from the experiments is much less clear, since several types of chemical ordering (both Co@Ag and reversed Ag@Co core-shell, Janus, multi-domains) were obtained depending on size, composition, temperature and growth conditions[25–29]. Recently, also long-lifetime metastable Ag nanoparticles with face-centered cubic structures including Co point defects have been obtained by laser ablation in liquid[30]. These results did not allow to determine which factors control the final structures, specifically they did not allow to disentangle equilibrium from kinetics effects, and to assess the influence of the environment.

In this work, we aim at determining the roles of equilibrium and kinetic effects in the formation of Co-Ag nanoparticles, which are grown on a weakly interacting substrate under UHV conditions to minimize the effects of the environment. This is very important especially for a metal such as cobalt which can be oxidised quite easily[31].

The originality of our approach is twofold. First, we use Graz-

[a] Interfaces, Confinement, Matériaux et Nanostructures, ICMN, Université d'Orléans, CNRS, Orléans, France.
[b] Synchrotron Soleil, Gif-sur-Yvette, France.
[c] Physics Department, University of Genoa, and CNR-IMEM, Genoa, Italy.
[d] MPQ, Université de Paris, CNRS, Paris, France.
[e] SP2M, ICMMO, Université Paris-Saclay, CNRS, Orsay, France.
* Corresponding author, e-mail Pascal.Andreazza@univ-orleans.fr.

† Electronic Supplementary Information (ESI) available: [details of any supplementary information available should be included here]. See DOI: 00.0000/00000000.

ing Incidence X-ray Scattering, at Small and Wide Angles (GISAXS and GIWAXS) in an innovative way, employing the anomalous mode to extract separately the contribution due to the whole particle and to Co atoms alone. In our GISAXS and GIWAXS experiments, the system is monitored *in situ* and in real time, so that growth is followed almost atom-by-atom. Second, we adopt a strongly out-of-equilibrium growth procedure, depositing Ag first, to produce an array of Ag nanoparticles, and subsequently depositing Co atoms on them. This may lead to the formation of the following structures:

(a) reversed Ag@Co core-shell, if Co atoms reach the surface of the Ag nanoparticles without entering inside them;

(b) mixed Co-Ag, initiated by Co atoms entering the Ag nanoparticles from random directions;

(c) Janus or quasi-Janus Co-Ag;

(d) Co@Ag core-shell.

Case (a) indicates the occurrence of strong kinetic trapping phenomena, so that nanoparticles are fully unable to achieve the equilibrium structure; (b) may correspond either to kinetic trapping phenomena or to nanoscale suppression of equilibrium phase separation, which has been theoretically predicted on the basis of the competition between mixing and interface free energies[32,33]. Scenarios (c) and (d) closely correspond to the equilibrium structures obtained in several simulations[16,17,24].

Our experimental results, interpreted with the aid of Monte Carlo (MC) and molecular dynamics (MD) simulations, will determine what is the most appropriate scenario, thanks to an almost atom-by-atom experimental resolution of the growth sequence.

2 Methods

A schematic representation of the experiments is given in Figure 1a. The Co-Ag NPs were obtained at room temperature (RT) by UHV vapor deposition on thermally oxidized Si(100) wafers covered by an amorphous carbon layer[34]. The deposition rates were between 0.5 to 1 10^{15} atoms/cm^2/h for each metal in an initial pressure of 1 10^{-10} mbar and an operating pressure 2 10^{-10} mbar during the deposition. These substrates were chosen to reduce the cluster-substrate interactions and to induce the formation of a randomly oriented assembly of isolated particles without preferential crystallographic orientation. Substrates were degassed at 500 K with a ramp rate of 10 K/min to clean the carbon layer (to vaporize water and some organic species).

An amount equivalent to 1.1 ML (monolayers as equivalent thickness) of Ag was deposited, on top of which 4.6 ML of Co were deposited. The composition of the nanoparticles assembly was calibrated before the experiment in similar conditions and also measured post-in situ experiment by an average method, the Rutherford backscattering (RBS), in order to check the composition ($\pm$5%) and the absolute quantity of deposited Co and Ag atoms. Previous experiments were performed to check the homogeneity of the composition in the level of each particle by energy dispersive spectroscopy (EDS) and the morphology of the initial Ag deposition in a transmission electron microscope (TEM) Jeol ARM200 (Figure S1).

GISAXS and GIWAXS experiments, in situ in UHV conditions, were carried out at the SIXS beam line at SOLEIL synchrotron. GISAXS measurements provide morphological features of a nanoparticle assembly as size, shape and correlation distance between particles on the substrate, while GIWAXS allows the determination of the nanoparticle structure at the atomic level[35,36].

From two different measurement campaigns, by using different photon energies (around 7700 eV and 16000 eV), incidence angles (but still close to the critical angles showed in Figure S2) and detection and resolution mode, several complementary sets of results were obtained (see the Supplementary Information (SI)). A campaign was focused on the end-of-deposition steps of the initial Ag particles and the deposition of the second metal, Co, in anomalous scattering (multiple energies) experimental configuration[37–39]. This is very powerful to reveal separately the scattering contribution of each atom type, but very costly in beam time and analysis time. The second campaign, devoted to the real-time monitoring of the morphology and the structure of nanoparticles during growth, was carried out under optimized conditions to obtain a sufficiently intense diffusion signal in a reduced acquisition time to simultaneously measure the scattered intensity at small and large angles, with a set of spectra collected every deposition of 5 atoms per cluster.

Monte Carlo (MC) and Molecular Dynamics (MD) numerical simulations were carried out using many-body interatomic potentials of the second moment tight-binding type[40,41]. Form and parameters of the potentials can be found in Refs. [16,17]. The validity of these potentials for AgCo nanoparticles has been validated against DFT calculations in Refs. [16].

Equilibrium MC simulations were done to obtain realistic structural models for analysing data obtained by GIWAXS. Indeed, even though MC and MD simulations should lead in principle to the same result, equilibrium MC simulations are freed from following physical trajectories in time and thus allow to reach the equilibrium state at a lower computational cost. These MC simulations are made in the canonical ensemble where the nominal concentration is kept fixed at a given temperature. A standard Metropolis algorithm is used[42] and the structural models for GIWAXS analysis consist in the last configuration obtained at T =300 K after 1 10^5 MC steps. A MC step corresponds to N propositions of a random atomic displacement and N propositions of a chemical switch obtained by exchanging the positions of two atoms with different chemical nature, N being the total (constant) number of atoms in the nanoparticle. We have verified for some configurations that they were similar to simulations using a larger number of MC steps.

MD simulations of the growth were done by depositing atoms one by one on the preformed seed[43,44], with rates of one atom every 5 or 10 ns (i.e. of 0.2 or 0.1 atoms/ns). The atoms were deposited from random directions. The starting position of each deposited atom was randomly chosen on a sphere centered on the growing cluster whose radius was larger by 0.6 nm than the maximum radius of the cluster. The initial velocity of the deposited atom was directed towards the cluster. The modulus of the initial velocity was extracted from a Maxwell distribution at the growth temperature. The equations of motion were solved by the velocity Verlet algorithm with a time step of 5 fs. Temperature was kept constant by an Andersen thermostat, whose collision frequency

(of 5 10^{11} s^{-1}) was chosen to ensure good thermalization with negligible perturbation of the dynamics[45].

3 Results

Here below we first analyze the final experimental structures obtained in the Ag deposition stage, and then after depositing Co atoms on top of them. This is followed by a real-time in situ analysis of growth stages in order to show how the nanoparticles evolve. These results will be discussed with reference to the (a-d) scenarios described in the Introduction. Finally, we analyze the atomic-level mechanisms of nanoparticle evolution by MD growth simulations.

3.1 Final structures of Ag seeds and of Co-Ag nanoparticles.

We now discuss the experimental results concerning the final structures of Ag seeds and of Co-Ag nanoparticles (Figures 1 and 2), obtained by GISAXS and GIWAXS measurements carried out at the end of Ag deposition and then towards the end of the subsequent Co deposition.

The fits of the in situ GISAXS data of Figure 1b-c (see the SI for the analysis procedure) allow to conclude that Ag deposition produced well-separated Ag clusters of ∼2 nm diameter. This is in agreement with the ex situ observation of similar samples by TEM imaging, as shown in Figures 1a and S1. These clusters were non-coalesced with an average separation between them of 3.5 nm.

Figure 2a shows two samples of Ag clusters of different average sizes, 1.9 and 2.8 nm. The experimental spectra are in very good agreement with a distribution of icosahedral structures, presenting however some structural disorder so that they are far from the perfect Mackay icosahedral model. The structures exhibit a mean contraction of atomic nearest-neighbour distances of 3% compared to the bulk crystal distances, due to the combination of the bond-length contraction caused by surface stress and of the core contraction which is always present in small icosahedral clusters[43,46,47].

The formation of a rather regular array of well-separated Ag aggregates on the substrate is an ideal situation for the subsequent deposition of Co atoms. We expect that these Co atoms land either on top of the Ag aggregates or on the substrate. In the latter case, we expect that Co atoms diffuse on the substrate to reach the aggregates and stick to them. This was indeed the case, as demonstrated by the GISAXS data of Figure 1, which show an increase in the clusters size but without much variation in the distance between them (3.5 nm).

From the analysis of the GISAXS q_x and q_z sections (by spectra simulations, see Supporting Information (SI)) at the end of Co deposition, we deduce the final size of the objects, which turns out to be ∼3 nm. The same analysis allows to eliminate scenario (a), because in Ag@Co nanoparticles the average thickness of the Co shell should be of 0.5 nm, which gives simulation spectra with high Co shell contribution, totally at odds with the experimental spectra. On the contrary, scenario (d) (Co@Ag core-shell) gives the best agreement with the experimantal data. However, we cannot conclude without ambiguity in favor of (d) at this stage of the analysis, because also mixed chemical ordering (scenario (b)) gives a satisfactory agreement (the data are not reported in the Figure). It is important to note that the GISAXS data are fitted with an average nanoparticle composition of $Co_{0.8}Ag_{0.2}$, in agreement with the composition measured ex situ by Rutherford backscattering after these synchrotron radiation experiments (see SI). In order to reach a firm conclusion about (d) vs (b), we analyze below the GIWAXS measurements (Figure 2) carried out in the anomalous mode, because they allow to extract the contribution of each element separately.

Figure 2b allows to qualitatively compare the GIWAXS spectrum obtained after Ag deposition with that obtained at the end of Co deposition. In the latter case, the contribution of Ag decreases and a new contribution appears at $q = 31$ nm^{-1}, which is positioned on the main contribution of metallic fcc cobalt. This observation is in agreement with the formation of a Co domain in the clusters. To extract the wide angle scattering contribution of Co atoms, anomalous scattering measurements (Figure 2c) were collected at five energies below the K Co absorption edge (7709 eV). The reference of the substrate signal was also measured at each energy. By a simplified PSF processing (see the SI) we extracted the anomalous contributions which is related only (or almost, according to the method) to Co (i.e. proportional to the partial scattering function $S(q)$ of Co-Co atom pairs, see the SI).

Figure 2d shows the contribution obtained by the differential method (subtraction of two signals obtained at different energies) and the raw experimental spectrum far from the K Co edge. This contribution is characteristic of a condensed phase of Co (with Co-Co distances very close to those of the bulk fcc phase of Co); it was compared to a calculated spectrum corresponding to a Co core of a Co@Ag particle of composition and size close to those of the experiment (923 atoms, $\simeq$ 3 nm). This particle, after optimization of the equilibrium structure by MC simulations, gives a scattering spectrum at large angles (Figure 2d) in very good agreement with the experimental spectrum.

In summary, the different analyses concur in singling out scenario (d) for the final state. This shows that the strongly non-equilibrium deposition of Co atoms on top of Ag nanoparticles finally produces Co@Ag structures, which are indeed quite close to the equilibrium structures found in several calculations[16,17]. The formation of Co@Ag structures is possible only by the migration of Co atoms inside the Ag clusters. We note also that the final Co@Ag structures may present incomplete Ag monolayer-thick shells[18,48] (often referred to as Ag-skins, Figure 2), because the quantity of Ag atoms is not sufficient to fully cover the Co core, even if the Ag shell is stretched to a monolayer thickness.

The experimental data allow us to conclude that Co@Ag structures are the final outcome of the growth. But what are the intermediate steps during the growth process? And what are the atomic-level mechanism involved in the formation of Co@Ag structures? To answer these questions, real-time growth experiments and cluster growth simulations are discussed below.

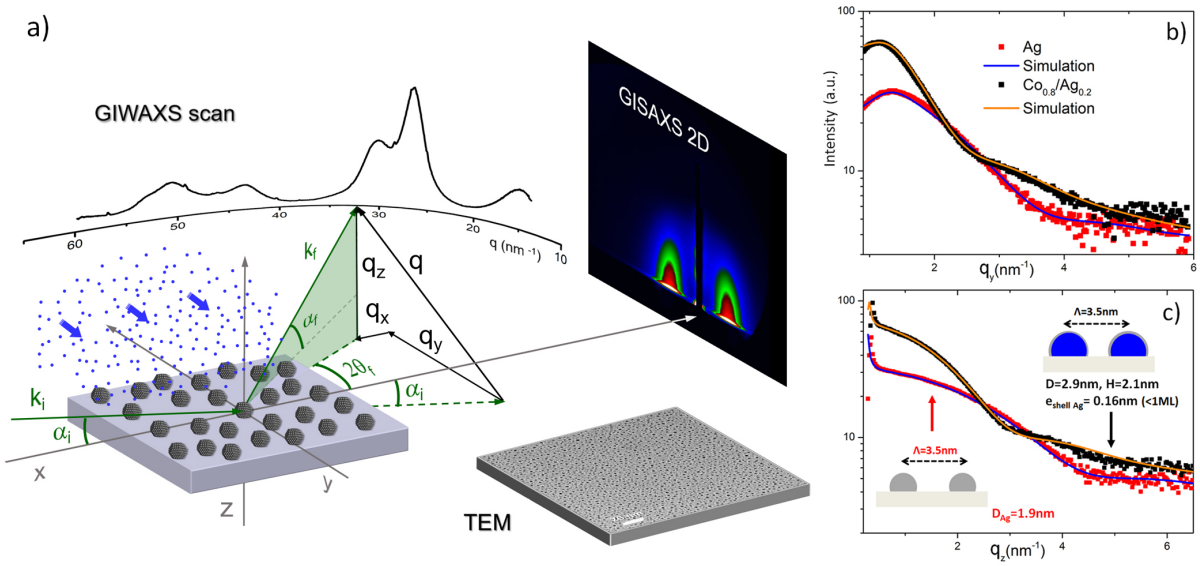

Fig. 1 a) Strategy of the scattering data collection with an incident beam of wavevector $\mathbf{k}_i$, a scattered beam in the direction $\mathbf{k}_f$ with respect to the sample and the 2D GISAXS and 0D GIWAXS detection geometry; in the inset, TEM image of an assembly of well-separated Ag clusters on amorphous carbon substrate (same deposition amount of Ag atoms in same conditions as the GISAXS/GIWAXS experiments). This micrograph is shown enlarged in Figure S1 for a better view. The white bar corresponds to the scale of 20 nm. b) Cross sections of 2D GISAXS spectra in the parallel direction and c) in the perpendicular direction to the substrate: initial NPs of Ag (in red), then NPs at the end of Co deposition (in black), as well as the profiles simulated by IsGISAXS (models for the simulations are shown in the inset graph c).

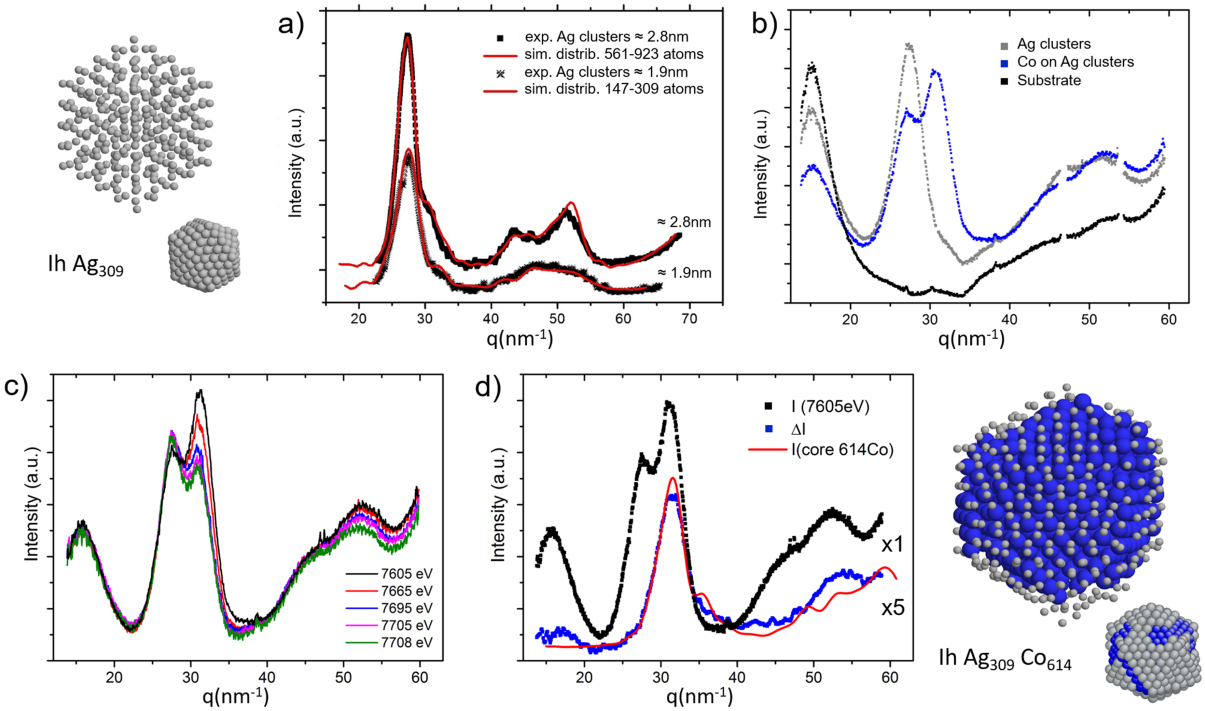

Fig. 2 GIWAXS spectra of a) two-size pure Ag nanoparticles with the superimposition of simulations of an Ih distribution; b) initial islets of Ag then after deposition of Co on Ag. Anomalous GIWAXS spectra obtained c) at different energies before the K Co edge; d) after extraction of the anomalous contribution of Co (differential method) superimposed with the simulated spectrum (in red) of a core of Co (b-c-d spectra are without substrate subtraction). The Ih structure models of Ag_{309} and $Ag_{309}Co_{614}$, after energy minimization by MC simulation, are included in a) and d), which correspond to the main sizes and concentrations of the initial islets of Ag and after deposition of Co, respectively. The Ag atoms are reduced in diameter to facilitate the view of Co atoms in the figure (Co in blue and Ag in gray).

3.2 Real-time investigation during Ag and Co deposition

The investigation of the intermediate growth steps was performed in real time by GISAXS and GIWAXS (see SI)[31,36]. This was carried out during Ag deposition and during that of Co, which were deposited with similar rates, of about one atom per minute per cluster. The GISAXS results (Figure 3(a-d)) reveal high mobility of Ag atoms on the substrate, up to a deposited amount equivalent to 1.1 ML, which results from an increase in the interparticle distances, in their diameters and heights (Figure 3c and d). In additiofaccurn, the aspect ratio changes from 0.89, corresponding to the initial nucleation step, to 0.82, corresponding to the growth step closer to the equilibrium of Ag supported clusters on a-C substrate. During Co deposition, up to 70% of deposited Co, the spectra show a stabilization of the interparticle distances, as revealed by the q position (1) in Figure 3b. On the other hand, the evolution of diameter and height shows a monotonic increase (Figure 3c and d), which validates the hypothesis that most Co atoms are able to diffuse on the substrate to reach the growing nanoparticles. From 70% Co onward, a sharp decrease in the aspect ratio H/D of the growing nanoparticles is observed (Figure 3d). This might correspond to a change of the substrate-metal interface caused by a change from an Ag-substrate interface to a Co-substrate interface. Above 70% Co, a jump in the interparticle distance Λ is also observed (Figure 3d, corresponding to the q position (2) in Figure 3b), indicating the occurrence of some static coalescence of the nanoparticles. In summary, below 70% Co, a model of non-coalesced growing Co@Ag nanoparticles can reasonably be proposed, whereas for larger quantities of deposited Co the situation is more complex. In the following we concentrate in the regime below 70% Co.

The GIWAXS results of Figure 4 reveal the time-resolved structural evolution during the Ag and Co depositions. The main feature is an intensity drop of the contribution of Ag-Ag pairs mainly around $q = 27.3\,\mathrm{nm}^{-1}$, which is associated with a loss of coherence of the Ag domains. At the same time, the formation of coherent Co domains is observed (Figure 4b), revealed by the increase of the scattering contributions from Co-Co pairs, which can be seen mainly around $q = 31.1\,\mathrm{nm}^{-1}$. More precisely, for 20% of deposited Co (Figure 4c - red circle), the signal assigned to Ag is stronger than that corresponding to the pure Ag clusters. This is the signature of an incorporation of Co atoms over interatomic distances close to that of Ag, while the structure of the initial Ag particles is mostly kept as it is. At the highest amounts of Co, the Ag atoms lose their coherence, corresponding to a shorter distance order in the initial Ag domains, while domains of Co are created close to the interatomic distance of Co bulk (within 1% of the bulk lattice spacing). The GISAXS spectra are showed in separated groups for a better view of the variation of the different contributions of Ag and Co in Figure S5. These observations, which reflect a progressive reduction of the coherence length in Ag domains and of the number of Ag neighbors, and also a higher local structural disorder, are in agreement with the model deduced from the anomalous scattering measurement: the formation of a core-shell Co@Ag particle by incorporation and agglomeration of Co atoms in the Ag nanoparticles.

3.3 Growth simulations

The experimental results were compared with MD growth simulations, in which Co atoms were deposited one by one from random directions on an initial Ag icosahedron of 309 atoms. This structure has a diameter $D \sim 2.2$ nm, which is in the size range of the experimental nanoparticles, see Figure 2a. A total of 700 Co atoms were deposited, at rates of 1 atom every 5 or 10 ns. Although MD simulations are not able to reach the experimental time scale, they have the advantage of reproducing realistic atomic trajectories because in these simulations the actual equations of motion are solved. In order to overcome these time scale limitations, we simulated at higher temperatures (500, 550 and 600 K) than in the experiments, so that a speed up of kinetics was obtained. These temperatures are however well below the melting temperature of the nanoparticles (which is above 700 K[49]) so that the simulated growth was always taking place at the solid state. For each temperature and deposition rate we made two independent simulations. We found that the growth sequence was of the same type in all simulations, a result which indicates that the simulations are indeed reproducing the typical growth pathway.

Representative snapshots from a growth sequence at 500 K with a deposition rate of 0.1 atom/ns are shown in Figure 5. The nanoparticle closely keeps the shape of the Ag icosahedron of 309 atoms up to ∼20% of Co content, in good agreement with the experiments. After reaching the nanoparticle, Co atoms may diffuse on its surface for some time, but then they are likely to enter the surface by exchange with Ag atoms, which are moved above the original surface to form islands on top of it. Local reconstructions of the surface are sometimes observed. These reconstructions allow a better accommodation of Co atoms at the surface. Co atoms initially occupy sites of the surface layer and then move to the sub-surface layer, filling the positions of the original Ag atoms. For isolated Co atoms in the sub-surface layer, the distances with Ag neighbours are quite close to those between sub-surface Ag-Ag pairs, with contractions in the range of 1-2%. For small sub-surface Co aggregates, distances with surrounding Ag atoms are more contracted, from about 3% of Co dimers to 5-6% for aggregates between 10 and 20 atoms. This result indicates that the experimental observation by GIWAXS in the first step of Co atom deposition (less than 20% of Co) corresponds to a sub-surface incorporation of Co atoms and consequently to the creation of Co-Ag pair distances close to the Ag-Ag pair distance.

An important point in the initial stages of the growth is that Co atoms or small Co aggregates, that are already present in the vicinity of the surface, act as traps for further deposited Co atoms that are diffusing on the cluster surface. This trapping effect is due to the much stronger Co-Co interactions compared to Ag-Co interactions. Because of this trapping effect, only few Co aggregates form, as shown in the first half of the sequence of Figure 5. These aggregate will further grow and eventually merge as the number of deposited Co atoms increases. We note also that these structures with sub-surface small aggregates do not correspond to the equilibrium chemical ordering in icosahedra in this composition range. In the equilibrium chemical ordering, the few Co

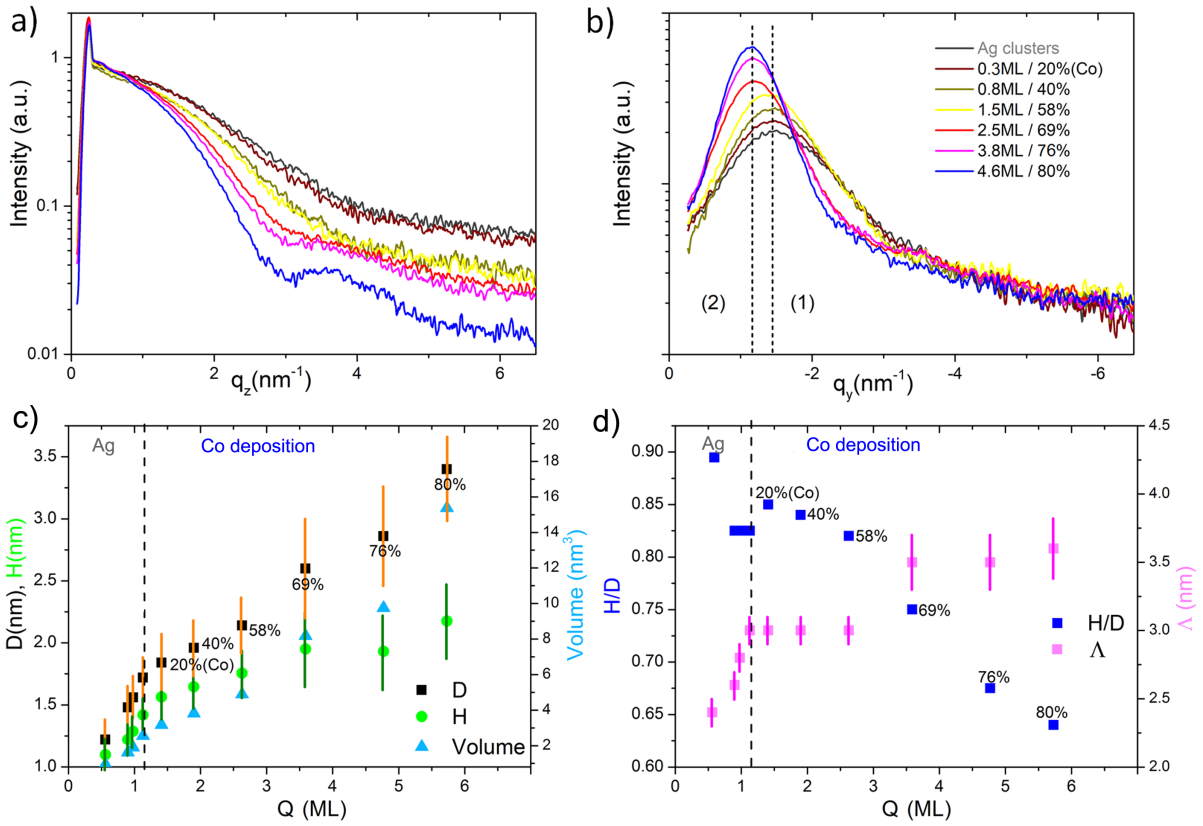

Fig. 3 GISAXS spectra during Co deposition: a) normalized on the intensity of the Yoneda peak in the q_z direction and b) raw in the q_y direction. Evolution of the average parameters (vertical bars correspond to the width σ of the Gaussian distributions): c) diameter D, height H and volume V, and d) aspect ratio (H/D) of the particles and interparticle distance (Λ) relative to the quantity of matter Q in equivalent thickness in monolayers (ML) of atoms.

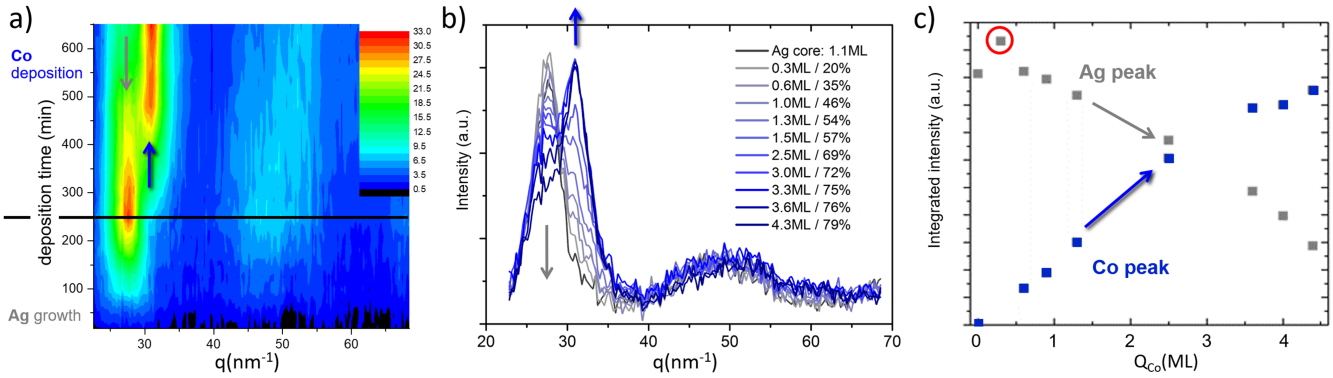

Fig. 4 a) GIWAXS spectra as a function of deposition time (the Ag and Co peaks are indicated by the gray and the blue arrows, respectively), the black horizontal line corresponding to the transition from the Ag to the Co deposition. b) Selection of a few spectra during Co deposition. These curves are shown separated and enlarged in Figure S5 for a better view. c) Integrated intensity of the main peaks assigned to Ag in gray and to Co in blue, located respectively around $q = 27.3$ nm^{-1} and $q = 31.1$ nm^{-1}.

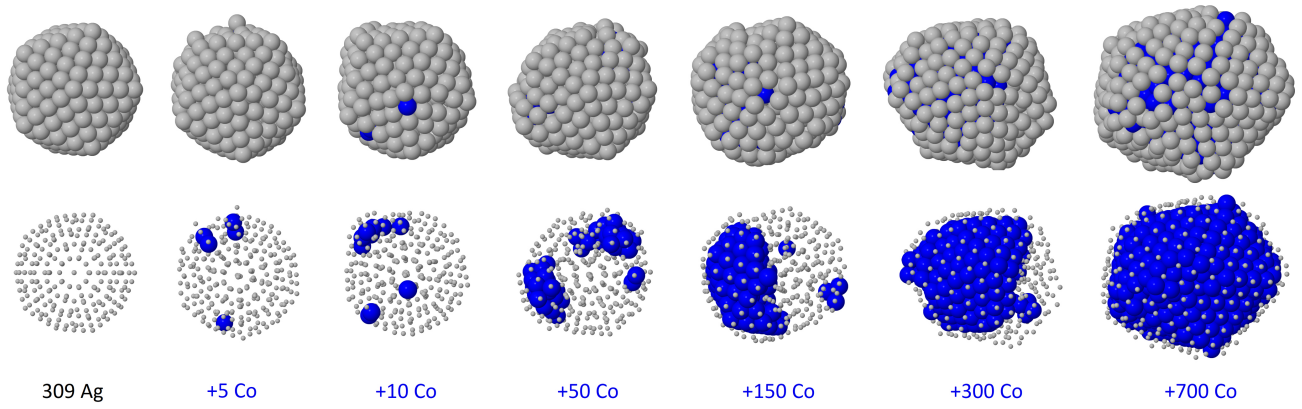

Fig. 5 Snapshots obtained by molecular dynamics simulations of the growth of Co on an initial Ag nanoparticle. The snapshots are taken at different stages representative of the process of incorporation of Co atoms up to 70% Co atom content. Co is in blue and Ag is in gray. The incorporation of Co in Ag keeps the original Ih shape at least up to 50 Co deposited atoms. The Ag atoms are reduced in diameter to facilitate the view of Co atoms in the bottom row of the figure. Note that Co atoms are deposited randomly from all directions.

atoms occupy the central part of the icosahedron, where they can release much of the internal stress of the structure [16,17]. However, sub-surface positions are relatively favorable from the energetic point of view, so that metastable configurations with small sub-surface Co aggregates may present long lifetimes. Specifically, sub-surface sites are the most favorable sites for placing small impurities in fcc clusters in systems such as AgCu, AgNi, AgCo, and AuCo, which present the same type of lattice mismatch, and of phase separation and surface segregation tendencies. The favourable sub-surface placement has been confirmed by DFT calculations for AgCu and AuCo [33,50]. In icosahedra, sub-surface sites are the second-best placements, after the central site.

By adding further Co atoms, the small sub-surface aggregates merge to form a single off-center cobalt block, which is covered on one side by an Ag-skin. This asymmetric quasi-Janus structure is obtained in spite of the fact that we deposit from completely random directions. The quasi-Janus structure is found up to about 400 deposited Co atoms and, according to calculations, it is close to the equilibrium chemical ordering for these compositions. [15–17] In agreement with our experiments, the structures then become Co@Ag for increasing Co content. We note that Co@Ag structures correspond to equilibrium in the Co-rich limit according to the calculations.

4 Conclusions

In summary, the growth of Co-Ag nanoparticles was followed in situ ad real time by different X-ray scattering techniques, with almost atom-by-atom resolution. The experimental results were interpreted with the aid of equilibrium Monte Carlo simulations and nanoparticle growth Molecular Dynamics simulations. This combination of techniques allowed to distinguish between different scenarios corresponding to possible different growth pathways and outcomes.

In particular, we show that the deposition of Co atoms on preformed Ag nanoparticles, which act as growth seeds, leads to quite complex growth sequences. These sequences start with the incorporation of Co atoms in sub-surface positions and finally end with the formation of Co@Ag core-shell arrangements. According to the growth simulations, this sequence passes through an intermediate stage in which quasi-Janus structures are formed. These structures present a Co core which is asymmetrically placed in the nanoparticle, so that it is covered on one side by a very thin Ag shell.

The observed growth sequences produce, to a large extent, structures which are close to what is expected for equilibrium Co-Ag nanoparticles [16,17], especially as regards the quasi-Janus structures at intermediate compositions and the Co@Ag structures in the Co-rich limit. These structures are obtained in spite of the fact that depositing Co atoms on Ag preformed nanoparticles is in principle a procedure very far from the expected equilibrium. The key atomic-level mechanism leading to equilibration is the fast incorporation of Co atoms inside the Ag seeds to reach the sub-surface positions, in which Co atoms are locally stable. According to our experimental results, this process is already activated at room temperature, and initiates the formation of Co aggregates inside the Ag matrix. As a result, kinetic trapping phenomena, which are however present in the initial part of the growth sequence, are of minor importance in determining the final growth outcomes.

Finally, we note that our results clearly demonstrate that in Co-Ag there is no nanoscale suppression of phase separation down to the limit of $\sim$3 nm at least, but well defined phase-separated types of chemical ordering such as core-shell and quasi-Janus structures are stable down to the extreme nanoscale limit.

Author Contributions

PA, CA and RF contributed to write the original draft; AC, YG, DN and JC contributed to review & editing. All authors contributed to the investigation: AL, CA, YG, AC, PA for experimental results and analysis; DN, JC and RF for simulation results.

Conflicts of interest

There are no conflicts to declare.

Acknowledgements

The authors are grateful to Bernard Legrand (CEA, saclay) for enthusiastic and helpful discussions. The authors acknowledge the SOLEIL (Gif sur Yvette, France) synchrotron facility for synchrotron radiation access and the SixS beamline team, in particular Michele Sauvage Simkin and Benjamin Voisin for technical help. RBS experiments were done at CEMHTI (Conditions Extrêmes et Matériaux: Hautes Temperatures et Irradiations, Orléans, France) This work was supported by the international research network IRN Nanoalloys of CNRS and the french Region council Centre-Val de Loire, Contract No. 201100070575.

Notes and references

1 R. Ferrando, J. Jellinek and R. L. Johnston, *Chem. Rev. (Washington, DC)*, 2008, **108**, 845–910.

2 R. Ferrando, *Structure and Properties of Nanoalloys*, Elsevier, 2016.

3 J. Jellinek, *Fadaray Discuss.*, 2008, **138**, 11–35.

4 P. Andreazza, V. Pierron-Bohnes, F. Tournus, C. Andreazza-Vignolle and V. Dupuis, *Surf. Sci. Rep.*, 2015, **70**, 188–258.

5 F. Y. Chen, B. C. Curley, G. Rossi and R. L. Johnston, *J. Phys. Chem C*, 2007, **111**, 9157–9165.

6 M. Zhang and R. Fournier, *J. Molec. Struct. {THEOCHEM}*, 2006, **762**, 49 – 56.

7 G. Barcaro, A. Fortunelli, M. Polak and L. Rubinovich, *Nano Lett.*, 2011, **11**, 1766–1769.

8 G. Rossi, A. Rapallo, C. Mottet, A. Fortunelli, F. Baletto and R. Ferrando, *Phys. Rev. Lett.*, 2004, **93**, 105503.

9 F. Baletto, C. Mottet and R. Ferrando, *Phys. Rev. Lett.*, 2003, **90**, 135504.

10 D. Ferrer, A. Torres-Castro, X. Gao, S. Sepúlveda-Guzmán, U. Ortiz-Méndez and M. José-Yacamán, *Nano Lett.*, 2007, **7**, 1701–1706.

11 J. M. Martinez De La Hoz, R. C. Tovar and P. B. Balbuena, *Mol. Sim.*, 2009, **35**, 785–794.

12 S. Nunez and R. L. Johnston, *J. Phys. Chem. C*, 2010, **114**, 13255–13266.

13 P. Grammatikopoulos, J. Kioseoglou, A. Galea, J. Vernieres, M. Benelmekki, R. E. Diaz and M. Sowwan, *Nanoscale*, 2016, **8**, 9780–9790.

14 M. Tchaplyguine, T. Andersson, C. Zhang and O. Björneholm, *J. Chem. Phys.*, 2013, **138**, 104303.

15 I. Parsina and F. Baletto, *J. Phys. Chem. C*, 2010, **114**, 1504–1511.

16 K. Laasonen, E. Panizon, D. Bochicchio and R. Ferrando, *J. Phys. Chem. C*, 2013, **117**, 26405–26413.

17 D. Bochicchio and R. Ferrando, *Phys. Rev. B*, 2013, **87**, 165435.

18 D. Nelli and R. Ferrando, *Nanoscale*, 2019, **11**, 13040–13050.

19 R. Sachan, S. Yadavali, N. Shirato, H. Krishna, V. Ramos, G. Duscher, S. J. Pennycook, A. K. Gangopadhyay, H. Garcia and R. Kalyanaraman, *Nanotechnology*, 2012, **23**, 275604.

20 V. Dupuis, A. Hillion, A. Robert, O. Loiselet, G. Khadra, P. Capiod, C. Albin, O. Boisron, D. Le Roy, L. Bardotti, F. Tournus and A. Tamion, *Journal of Nanoparticle Research*, 2018, **20**, 128.

21 I. Karakaya and W. T. Thompson, *Bull. Alloy Phase Diagrams*, 1986, **8**, 259–263.

22 L. Vitos, A. Rubana, H. Skrivera and J. Kollár, *Surface Science*, 1998, **411**, 186 – 202.

23 T. van Hoof and M. Hou, *Phys. Rev. B*, 2005, **72**, 115434.

24 G. Rossi, G. Schiappelli and R. Ferrando, *J. Comput. Theor. Nanosci.*, 2009, **6**, 841.

25 L. Favre, S. Stanescu, V. Dupuis, E. Bernstein, T. Epicier, P. Mélinon and A. Perez, *Appl. Surf. Sci.*, 2004, **226**, 265–270.

26 J. Tuaillon-Combes, O. Boisron, E. Bernstein, G. Guiraud, A. Gerbert, A. Milner, P. Mélinon and A. Perez, *Appl. Surf. Sci.*, 2004, **226**, 321–326.

27 M. Gaudry, E. Cottancin, M. Pellarin, J. Lermé, L. Arnaud, J. R. Huntzinger, J. L. Vialle, M. Broyer, J. L. Rousset, M. Treilleux and P. Mélinon, *Phys. Rev. B*, 2003, **67**, 155409.

28 J. Garcia-Torres, E. Vallés and E. Gómez, *Journal of Nanoparticle Research*, 2010, **12**, 2189–2199.

29 R. Sachan, A. Malasi, S. Yadavali, B. Griffey, J. Dunlap, G. Duscher and R. Kalyanaraman, *Particle & Particle Systems Characterization*, 2015, **32**, 476–482.

30 A. Guadagnini, S. Agnoli, D. Badocco, P. Pastore, D. Coral, M. B. Fernàndez van Raap, D. Forrer and V. Amendola, *Journal of Colloid and Interface Science*, 2021, **585**, 267 – 275.

31 J. Penuelas, P. Andreazza, C. Andreazza-Vignolle, H. Tolentino, M. D. Santis and C. Mottet, *Phys. Rev. Lett.*, 2008, **100**, 115502.

32 A. Christensen, P. Stolze and J. K. Nørskov, *J. Phys. Condens. Matter*, 1995, **7**, 1047.

33 J.-P. Palomares-Baez, E. Panizon and R. Ferrando, *Nano Letters*, 2017, **17**, 5394–5401.

34 J. Penuelas, C. Andreazza-Vignolle, P. Andreazza, A. Ouerghi and N. Bouet, *Surf. Sci.*, 2008, **545-551**,.

35 P. Andreazza, *Probing Nanoalloy Structure and Morphology by X-Ray Scattering Methods*, 2012, In *Nanoalloys – Synthesis, Structure and Properties*, pages 69-112 . Edited by D. Alloyeau, C. Mottet and C. Ricolleau. Springer Verlag, Berlin.

36 J. Penuelas, P. Andreazza, C. Andreazza-Vignolle, C. Mottet, M. De Santis and H. C. N. Tolentino, *The European Physical Journal Special Topics*, 2009, **167**, 19–25.

37 P. Andreazza, H. Khelfane, O. Lyon, C. Andreazza-Vignolle, A. Ramos and M. Samah, *Eur. Phys. J. Spec. Top.*, 2012, **208**, 231–244.

38 C. Yu, S. Koh, J. Leisch, M. Toney and P. Strasser, *Faraday Discussions*, 2008, **140**, 283–296.

39 U. Jeng, Y. Lai, H. Sheu, J. Lee, Y. Sun, W. Chuang, Y. Huang and D. Liu, *J. Appl. Crystallogr.*, 2007, **40**, 418422.

40 F. Cyrot-Lackmann and F. Ducastelle, *Phys. Rev. B*, 1971, **4**, 2406–2412.

41 V. Rosato, M. Guillopé and B. Legrand, *Phil. Mag. A*, 1989, **59**, 321.

42 K. Binder, *The Monte Carlo Method in Condensed Matter Physics*, Springer Verlag, Berlin, 1995.

43 F. Baletto, C. Mottet and R. Ferrando, *Phys. Rev. B*, 2001, **63**, 155408.
44 D. M. Wells, G. Rossi, R. Ferrando and R. E. Palmer, *Nanoscale*, 2015, **7**, 6498–6504.
45 F. Baletto, C. Mottet and R. Ferrando, *Surf. Sci.*, 2000, **446**, 31–45.
46 P. A. Montano, W. Schulze, B. Tesche, G. K. Shenoy and T. I. Morrison, *Phys. Rev. B*, 1984, **30**, 672–677.
47 R. Lamber, S. Wetjen and N. I. Jaeger, *Phys. Rev. B*, 1995, **51**, 10968–10971.
48 E. Panizon and R. Ferrando, *Nanoscale*, 2016, **8**, 15911–15919.
49 C. Mottet, G. Rossi, F. Baletto and R. Ferrando, *Phys. Rev. Lett.*, 2005, **95**, 035501.
50 D. Bochicchio and R. Ferrando, *Nano Lett.*, 2010, **10**, 4211–4216.